

# Inclusive Two-Jet Production at HERA: Direct and Resolved Cross Sections in Next-to-Leading Order QCD

M. Klasen\*, G. Kramer  
II. Institut für Theoretische Physik†  
Universität Hamburg  
D - 22761 Hamburg, Germany

## Abstract

We have calculated inclusive two-jet cross sections in next-to-leading order QCD for low  $Q^2$   $ep$  collisions superimposing direct and resolved contributions. Infrared and collinear singularities in the virtual and real contributions are cancelled with the phase space slicing method. Various inclusive two-jet distributions have been computed. The results are compared with recent data from the ZEUS collaboration at HERA.

---

\*Now at Deutsches Elektronen-Synchrotron (DESY), Notkestraße 85, D-22607 Hamburg, Germany.

†Supported by Bundesministerium für Forschung und Technologie, Bonn, Germany under Contract 05 7HH92P(0) and EEC Program "Human Capital and Mobility" through Network "Physics at High Energy Colliders" under Contract CHRX-CT93-0357 (DG12 COMA)

# 1 Introduction

The analysis of large transverse energy ( $E_T$ ) jets produced in  $ep$  scattering with very small virtuality ( $Q^2 \simeq 0$ ) offers the possibility to learn about the partonic structure of real photons. The hard momentum scale  $E_T$  allows the application of perturbative QCD to predict cross sections for the production of two or more high- $E_T$  jets.

As is well known, in lowest order (LO) QCD two distinct processes contribute to the hard scattering cross sections. In the direct process, the incoming photon interacts in a point-like fashion with the quark from the proton via the QCD Compton scattering  $\gamma q \rightarrow gq$  or via the photon-gluon fusion process  $\gamma g \rightarrow q\bar{q}$ , if a gluon comes out of the proton. In the resolved process, the photon acts as a source of partons, which can scatter off the partons in the proton. Therefore, the cross section for the resolved process depends on the parton distributions in the photon in addition to the parton distribution functions in the proton.

The two processes have distinctly different event structures. Whereas the direct process results in events with a characteristic (2+1)-jet structure, i.e. two high- $E_T$  jets and one low- $E_T$  remnant jet from the proton, the resolved photon events have a characteristic (2+2)-jet structure, where in addition to the two high- $E_T$  jets and the low- $E_T$  proton remnant a second jet of low- $E_T$  fragments of the photon is produced. While in the (2+1)-jet events the total photon energy contributes to the hard scattering process, only a fraction participates in the (2+2)-jet events.

This characterization of the direct and resolved processes is valid only in LO. In next-to-leading order (NLO), the direct cross section may also have contributions with a photon remnant jet. In addition, both components are related to each other through the factorization scheme and scale at the photon leg. The dependence of the NLO direct cross section on this scheme/scale must cancel up to NNLO terms against the scheme/scale dependence of the resolved cross section. Therefore in NLO both components must be considered together and consistently be calculated up to NLO in the parton distributions of the photon and the proton, respectively, and in the hard scattering cross sections.

The simplest observable is the inclusive single-jet cross section. It depends on the transverse energy and the rapidity of the observed jet. Complete NLO calculations for this cross section have been done previously [1, 2, 3] and have been compared to experimental data from ZEUS [4] and H1 [5]. In these calculations special techniques for cancelling soft and collinear singularities have been applied, which are suitable only for the computation of inclusive single-jet cross sections. To obtain different cross sections, as for example the inclusive two-jet cross section, the whole calculation must be repeated. Inclusive two-jet cross sections depend on one more variable. Therefore they are a much more stringent test of the QCD predictions than inclusive single-jet cross sections. Furthermore, for a comparison with experimental data the calculations must be performed in such a way that the experimental cuts can be built in easily. For this purpose, the so-called phase space slicing method is suited particularly well. In this method, an invariant mass resolution cut is introduced to isolate the soft and collinear singularities of initial and final states. This resolution cut is purely technical and is chosen small enough not to disturb any experimental constraints or jet recombination requirements. Based on this method we recently calculated the inclusive two-jet cross section for direct photoproduction [6].

The results of this calculation were compared with data from the ZEUS collaboration [7], in which the direct contribution and the resolved contribution were separated with a cut on  $x_\gamma$ , i.e. the momentum fraction of the photon entering the hard scattering. The contribution of the resolved photon in the enriched direct  $\gamma$  sample was estimated in lowest order since it was supposed to contribute only a fraction in this sample. As a result of this investigation it turned out that the resolved contribution in the enriched direct  $\gamma$  sample was not negligible and could be, depending on the assumed photon structure function, as large as 30% of the total two-jet cross section. It is clear that the estimate of the resolved cross section in this region by a LO computation is insufficient and that the NLO corrections of the resolved cross section must be included. In addition, in the same analysis of the ZEUS two-jet data [7] the inclusive two-jet cross section in an enriched resolved  $\gamma$  sample was measured, which could be a decisive test of the available parton distributions of the photon. For this reason and since we expect more two-jet experimental data in the future, a complete NLO calculation of the inclusive two-jet cross section is mandatory. For the direct component, we rely on our previous work [6, 8]. The NLO calculation of the resolved component has been completed recently [9]. A detailed description of the calculation will be presented in a separate publication [10]. Here we shall only give a short presentation, report some results on various inclusive two-jet cross sections, which might be measured in the future, and recalculate the two-jet cross section in the enriched direct  $\gamma$  sample and the enriched resolved  $\gamma$  sample for a comparison with recent ZEUS data [11].

The outline of the paper is as follows: in section 2, we explain the formalism used to calculate the inclusive two-jet cross section for the resolved part. In section 3, we present some results in order to demonstrate the flexibility of our method and a comparison with recent ZEUS measurements. Section 4 contains a summary.

## 2 Next-To-Leading Order Cross Sections

### 2.1 Photon Spectrum

Before we explain how the NLO corrections have been calculated, we must specify the relation between the  $ep$  and the  $\gamma p$  cross sections. Let us start with the electroproduction process

$$e(k) + p(p) \rightarrow e'(k') + X, \quad (1)$$

where  $k$ ,  $k'$ , and  $p$  are the four-momenta of the incoming and outgoing electron (positron) and the proton, respectively.  $X$  denotes a generic hadronic system which will be specified later.  $q = k - k'$  is the momentum transfer of the electron to the photon with virtuality  $Q^2 = -q^2 \simeq 0$ . For small  $Q^2$ , the  $ep$  cross section can be calculated in the Weizsäcker-Williams approximation, where the  $\gamma p$  cross section can be factorized and the photon spectrum is given by the function

$$F_{\gamma/e}(x_a) = \frac{\alpha}{2\pi} \frac{1 + (1 - x_a)^2}{x_a} \ln \frac{Q_{\max}^2 (1 - x_a)}{m_e^2 x_a^2}. \quad (2)$$

Here,  $m_e$  is the electron mass, and  $x_a = (pq)/(pk) \simeq E_\gamma/E_e$  is the fraction of the initial electron energy transferred to the photon. The cross section for the process (1)  $ep \rightarrow e'X$  is then given by the convolution

$$d\sigma(ep \rightarrow e'X) = \int_{x_{a,\min}}^{x_{a,\max}} dx_a F_{\gamma/e}(x_a) d\sigma(\gamma p \rightarrow X). \quad (3)$$

$Q_{\text{max}}^2$ ,  $x_{a,\text{max}} \leq 1$ , and  $x_{a,\text{min}}$  are determined by the tagging conditions of the experiments at HERA and will be specified when we present our numerical results. In (3),  $d\sigma(\gamma p \rightarrow X)$  is the photoproduction cross section with initial photon energy  $E_\gamma = x_a E_e$  and photon virtuality  $Q^2 \simeq 0$ .

## 2.2 Jet Cross Sections in NLO

As we explained in the introduction, inclusive jet cross sections  $d\sigma(\gamma p \rightarrow \text{jets})$  receive contributions from two components, direct and resolved, depending on the way in which the incoming photons participate in the hard scattering subprocesses. In the resolved case, the NLO inclusive two-jet cross section is calculated from the formula

$$\frac{d^3\sigma}{dE_T d\eta_1 d\eta_2} = \sum_{a,b=q,g} \int dy_a \int dx_b F_{a/\gamma}(y_a, M_\gamma^2) F_{b/p}(x_b, M_p^2) \left\{ \left( \frac{d^3\sigma(ab \rightarrow \text{jet}_1 + \text{jet}_2)}{dE_T d\eta_1 d\eta_2} \right)_{\text{LO}} + \frac{\alpha_s(\mu)}{2\pi} K_{ab}(R, M_\gamma, M_p, \mu) \right\}. \quad (4)$$

In (4),  $E_T$  is the transverse energy of the measured or trigger jet with rapidity  $\eta_1$ .  $\eta_2$  denotes the rapidity of another jet such that in the three-jet sample these two jets have the largest and second largest  $E_T$ , i.e.  $E_{T_1}, E_{T_2} > E_{T_3}$ . The first term on the right-hand side of (4) is the LO cross section, and the second term is the NLO correction. The latter depends on the factorization scales  $M_\gamma$  and  $M_p$  at the photon and proton vertex, at which the initial state singularities are absorbed into the parton distribution functions of the photon and the proton.  $\mu$  is the renormalization scale. The variable  $R$  is the usual cone size parameter, which defines the size of the jets with transverse energy  $E_T$ , rapidity  $\eta$ , and azimuthal angle  $\phi$ . When two partons fulfill the Snowmass condition [12] with the cone size parameter  $R$ , they are combined into one jet. The same jet definition must be used in the analysis of the experimental data, if a meaningful comparison between theory and experiment is intended. It is clear that either of the two jets can consist of two partons inside a cone with radius  $R$ . Essentially the same formula applies for the direct cross section. In this case, the photon structure function  $F_{a/\gamma}(y_a, M_\gamma^2)$  is replaced by  $\delta(1 - y_a)$ .

The NLO corrections  $K_{ab}$  in (4) for the hard scattering subprocesses are calculated with the phase space slicing method using an invariant mass cut for the separation of the cross section for  $\gamma p \rightarrow 2$  jets and  $\gamma p \rightarrow 3$  jets. This invariant mass cut is defined by  $2p_i p_j < ys$ , where  $s$  is the partonic center-of-mass energy squared. So, for example, in the resolved subprocess  $q_i \bar{q}_j \rightarrow q_i \bar{q}_j g$ , where  $q_i, q_j$  can be identical or non-identical quarks, the cross section has soft, initial, and final state collinear singularities. The cross section  $d\sigma(q_i \bar{q}_j \rightarrow q_i \bar{q}_j g)$  is integrated over these singular regions up to the cut-off  $y$ , which isolates the respective singularities in terms of poles in  $\varepsilon = (4 - d)/2$ , where  $d$  is the dimension in the dimensional regularization method. These singularities cancel against the singular contributions of the virtual corrections to  $q_i \bar{q}_j \rightarrow q_i \bar{q}_j$  and against the subtraction terms at the scales  $M_\gamma$  and  $M_p$ , which are absorbed into the parton distribution functions of the photon and the proton, respectively. Outside the cut-off region, i.e. for  $2p_i p_j > ys$ , we have genuine  $q_i \bar{q}_j g$  final states. The cross section in this region is subdivided into the two-jet cross section and the three-jet cross section contribution, depending on whether two of the final state partons are combined according to the Snowmass condition or not. The LO contribution, the NLO virtual contributions, and the NLO corrections inside the  $y$ -cut contribute to the two-jet cross section together with the contributions

inside the recombination cone with radius  $R$ . The part of the  $q_i\bar{q}_jg$  cross section not fulfilling the cone recombination condition is the three-jet cross section, from which we have calculated the inclusive two-jet cross section as a function of  $E_T$ ,  $\eta_1$ , and  $\eta_2$ . For the exclusive two-jet cross section,  $E_{T_1} = E_{T_2} = E_T$ . To separate double singularities in the  $q_i\bar{q}_jg$  cross section part we have used the method of partial fractioning. The same partial fractioned expressions are applied for the calculation inside and outside the  $y$ -cut. Inside the  $y$ -cut region, the integrations are done analytically with the approximation that terms  $\mathcal{O}(y)$  are neglected. This is necessary since otherwise with a  $d$ -dimensional space-time the necessary integration could not be carried out. Outside the  $y$ -cut region, the contributions to the inclusive cross section are evaluated with no further approximations. Because of the approximation in the analytic part inside the  $y$ -cut, the parameter  $y$  must be chosen very small. It turned out that for  $y$  of the order  $10^{-3}$  to  $10^{-4}$  the inclusive cross section is independent of the cut-off parameter  $y$ . However, the inclusive two-jet cross section depends on the cone size  $R$ , which must be chosen in accordance with the analysis of the experimental data. In the case of all the other hard subprocesses for the resolved cross section, of which there are many and which will not be listed here, the calculation proceeds in the same way. The complete list will be given in a separate publication [10] and can also be found in [9, 13]. In these references, the details of the analytic integrations and the cancellation of the singularities for NLO corrections is described as well. For the direct cross section, the calculation of the NLO correction was already reported and is given with all details in our previous work [6, 8, 9].

Before the final results were obtained, some tests of the NLO corrections have been performed. For similar tests of the NLO corrections of the direct cross section see [6]. The same tests were done for the resolved subprocesses. So we checked that the cross sections are independent of the cut-off  $y$  if  $y$  is chosen small enough. This was the case for  $y \leq 10^{-3}$  in all considered cases under different kinematical conditions. For  $y > 10^{-3}$ , we observed some small  $y$  dependence caused by the approximations in the analytical integrations. Second, the resolved inclusive one-jet cross section was calculated and compared with earlier results for which a completely different method for cancelling the infrared and collinear singularities was applied [2, 14]. Very good agreement was found in all channels and for the total resolved cross section. Third we tested that the sum of the NLO direct and the LO resolved cross section is independent of the factorization scale  $M_\gamma$  similar to such a test for the single-jet inclusive cross section earlier [15]. Details of these tests can be found in [9].

For the calculation of the inclusive jet cross sections, we need the parton distributions  $F_{a/\gamma}$  of the photon and  $F_{b/p}$  of the proton, respectively (see (4)). We have chosen the NLO set of Glück, Reya, and Vogt (GRV) in the  $\overline{\text{MS}}$  scheme for  $F_{a/\gamma}$  [16] and the CTEQ3M set, i.e. also a  $\overline{\text{MS}}$  set in NLO, for  $F_{b/p}$  [17]. All scales are set to  $\mu = M_\gamma = M_p = E_T$ .  $\alpha_s$  is calculated from the two-loop formula with  $n_f = 4$  massless flavors with  $\Lambda_{\overline{\text{MS}}}^{(4)} = 239$  MeV, equal to the  $\Lambda$ -value of the CTEQ3M parton distributions. The charm quarks are treated as light flavors with the boundary condition that the charm content of the two structure functions vanishes for  $M_\gamma^2, M_p^2 < m_c^2$  with  $m_c = 1.5$  GeV.

### 3 Results and Comparison with ZEUS Data

In this section we present some characteristic numerical results for two-jet cross sections concentrating on the resolved contribution. All results are obtained with the phase space slicing method. Except where we compare with recent ZEUS data, we do not apply special cuts on kinematical variables of the initial or final states dictated by the experimental analysis, although this is necessary if one wants to confront the prediction with experimental data. Therefore, the photon energy fraction  $x_a$  in (2) is allowed to vary in the kinematically allowed range from  $x_{a,\min} \leq x_a \leq 1$ .  $Q_{\max}^2 = 4 \text{ GeV}^2$  in (2) is the same as usually used in the jet analysis of the ZEUS experiment.

The further evaluation of the two-jet cross section is based on two separate contributions – a set of two-body contributions and a set of three body contributions. Each set is completely finite, as all singularities have been cancelled or absorbed into structure functions in the same way as in the case of the direct cross section [8]. Each part depends separately on the cut-off  $y$ . The analytic contributions are valid only for very small  $y$ , since terms of  $\mathcal{O}(y)$  have been neglected. For very small  $y$ , the two contributions have no physical meaning. In this case, the terms depending on  $\ln y$  force the two-body contributions to become negative, whereas the three-body cross sections are large and positive. The resolved cross section shows a similar behavior [9]. When the two- and three-body contributions are superimposed to yield the inclusive two-jet cross section, the dependence on the cut-off will cancel. This will only be the case if the inclusive cross sections are defined in the correct way, so that they are infrared safe. We have checked this explicitly by varying  $y$  in the superposition of the two pieces for the inclusive one-jet and two-jet cross section separately. For the two-jet cross section, it is essential that the variable  $E_T$  is chosen in the way as stated above, namely that  $E_T$  is the transverse momentum of the two largest  $E_T$  jets. This means that the cut-off  $y$  is purely technical. It only serves to distinguish the phase space regions, where the integrations are done analytically with arbitrary dimensions from those where they are done numerically in four dimensions. When one compares to experimental data with special kinematical cuts,  $y$  must be chosen sufficiently small in order to make sure that the cuts on kinematical variables of the final state do not interfere with the cancellation of the  $y$  dependence.

For the recombination of two partons  $i$  and  $j$  with the cone constraint  $R_{i,j} < R$ , where

$$R_i = \sqrt{(\eta_i - \eta_j)^2 + (\phi_i - \phi_j)^2} \quad (5)$$

and  $\eta_j, \phi_j$  are the rapidity and azimuthal angle of the recombined jet, we choose the radius  $R = 1$ . In some cases, an ambiguity may occur when two partons  $i$  and  $j$  qualify both as two individual jets  $i$  and  $j$  and as a combined jet. In this case we only count the combined jet to avoid possible double counting. It is clear that in NLO the final state may consist of two or three jets. The three-jet sample consists of all three-body contributions, which do not fulfill the cone constraint given above.

First we show results for the resolved inclusive two-jet cross section in fig. 1. We fixed  $\eta_1$  at  $\eta_1 = 1$  and  $\eta_2$  at three different values of  $\eta_2 = 0, 1, 2$  and plot the cross section as a function of  $E_T = E_{T_1}$ . The curves for  $\eta_2 = 0$  and  $\eta_2 = 2$  are rescaled by factors of 0.1 and 0.5. Since the two-jet cross section is much more exclusive than the one-jet cross section, it is reduced in magnitude as we expect it. In fig. 1, we also show the LO cross section as a function of  $E_{T_1}$ .

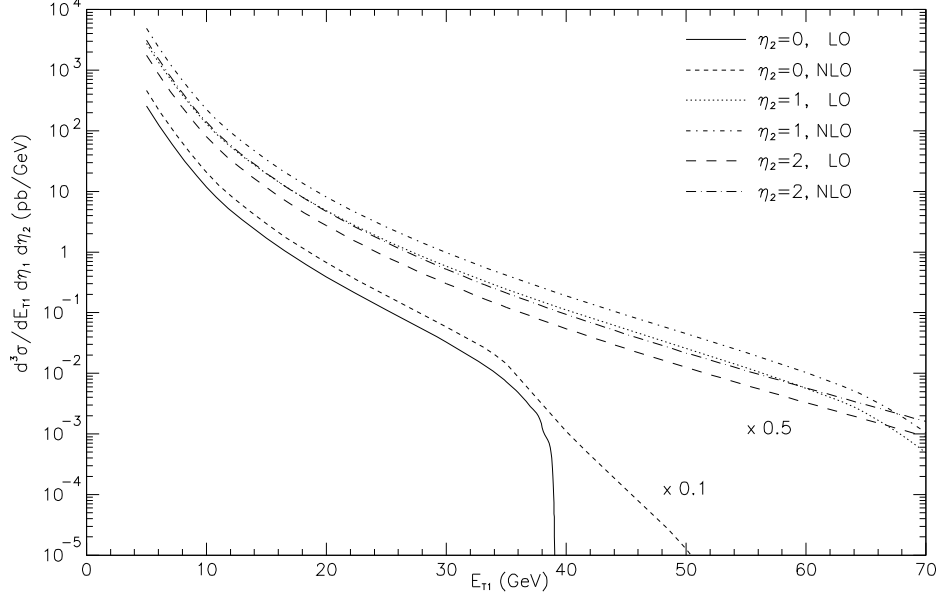


Figure 1: *Inclusive dijet cross section  $d^3\sigma/dE_{T_1}d\eta_1d\eta_2$  for resolved photons as a function of  $E_{T_1}$  for  $\eta_1 = 1$  and three values of  $\eta_2 = 0, 1, 2$ . The cross section for  $\eta_2 = 0$  ( $\eta_2 = 2$ ) is multiplied by 0.1 (0.5).*

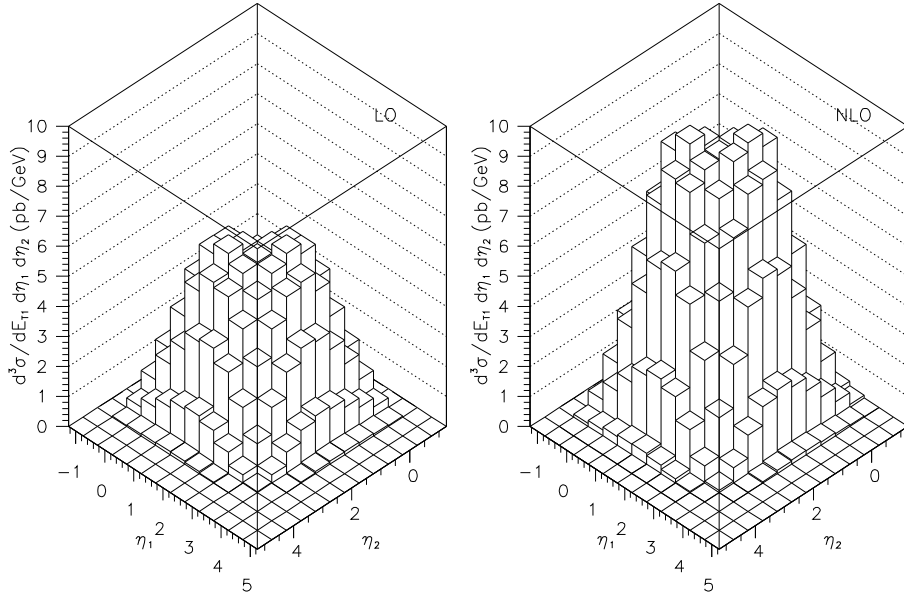


Figure 2: *Inclusive dijet cross section  $d^3\sigma/dE_{T_1}d\eta_1d\eta_2$  at  $E_{T_1} = 20$  GeV for resolved photons, as a function of  $\eta_1$  and  $\eta_2$ . The LO plot (left) is exactly symmetric, the NLO plot (right) only approximately.*

The ratio of NLO to LO is 1.7 over the whole  $E_{T_1}$  range. In this comparison, the LO cross section is calculated with the LO subprocesses, but with the same definition of  $\alpha_s$  and NLO structure functions. For  $\eta_2 = 0$  the NLO and LO differ very much for large  $E_{T_1}$ . In this case the third jet in NLO opens up additional phase space, so that  $E_{T_1}$  can go up to  $E_{T_1} < 50$  GeV. A similar behavior is observed for the corresponding direct cross section shown in [8].

Next we present the dependence of the resolved cross section on the two rapidities in form of the three-dimensional lego-plots in fig. 2. The equivalent plot for the direct cross section was already given in [8]. The leading order is shown on the left side and is completely symmetric in  $\eta_1$  and  $\eta_2$ . The NLO cross section, which is shown on the right-hand side of fig. 2, is not symmetric any more due to the presence of a trigger jet with transverse energy  $E_{T_1}$ , which is fixed at  $E_{T_1} = 20$  GeV. This can best be seen at the bottom of the contour plots, where at least one of the two observed jets is far off the central region. The NLO predictions are considerably larger than the LO predictions. For the direct cross section, the NLO cross section is only moderately larger than the LO cross section [8], where the  $k$ -factor is 1.25.

This becomes even clearer when we plot the projections of the lego-plots for fixed  $\eta_1 = 0, 1, 2$  and 3. In fig. 3, the LO and NLO distributions in  $\eta_2$  are shown for the direct photoproduction and in fig. 4 for the resolved part. In the direct case it is clearly seen that the second jet tends to be back-to-back with the first jet, since the maximum always occurs at  $\eta_2 \simeq \eta_1$ . However, at  $\eta_1 = 3$  this is no longer possible due to phase space restrictions. The  $\eta_2$ -distributions for resolved photons in fig. 4 are considerably broader than in fig. 3 due to the smearing of the hard cross sections with the distribution functions of the partons in the photon. The maxima of the curves are also not so much dominated by kinematics but more by the quark and gluon structure of the photon in different  $x_\gamma$  regimes. They do not lie at  $\eta_2 = \eta_1$ . Therefore, two-jet rapidity distributions are very well suited to constrain the photon structure. The  $k$ -factors range from 1.65 to more than 3 in the very forward region of the proton. The shapes of the distributions are very similar in LO and NLO. The absolute values make, however, an important difference.

Next we show the sum of the direct and resolved cross sections which gives the physical complete photoproduction result. First we have plotted the two-jet cross section as a function of the transverse energy  $E_{T_1}$  at  $\eta_1 = \eta_2 = 1$ . Fig. 5 gives the LO result, fig. 6 the NLO result. As we can see, the point where direct and resolved contributions are equally important is near  $E_{T_1} = 20$  GeV in leading order and  $E_{T_1} = 30$  GeV in next-to-leading order. These crossing points are somewhat smaller than for the inclusive one-jet cross section at  $\eta = 1$ , so that direct photons make a stronger impact in dijet production.

If one plots the complete two-jet cross sections as a function of  $\eta_2$ , the different behaviors of direct and resolved photons add up to the full curves in fig. 7 (LO) and fig. 8 (NLO). These plots are best suited to decide in which rapidity regions one can see best the resolved photon structure. We have already seen that this will be in situations where the two jets are not back-to-back, e.g. for  $\eta_1 = 0$  and positive  $\eta_2$  in the upper left plots of fig. 7 and 8. On the other hand, the proton structure can best be studied with direct photons, when the cross section is not folded with another distribution. A possibility is at  $\eta_1 = 0$  and negative values of  $\eta_2$ . This is especially interesting for the small- $x$  components of the proton like the gluon and the quark sea. Another interesting observation is that the relative importance of direct

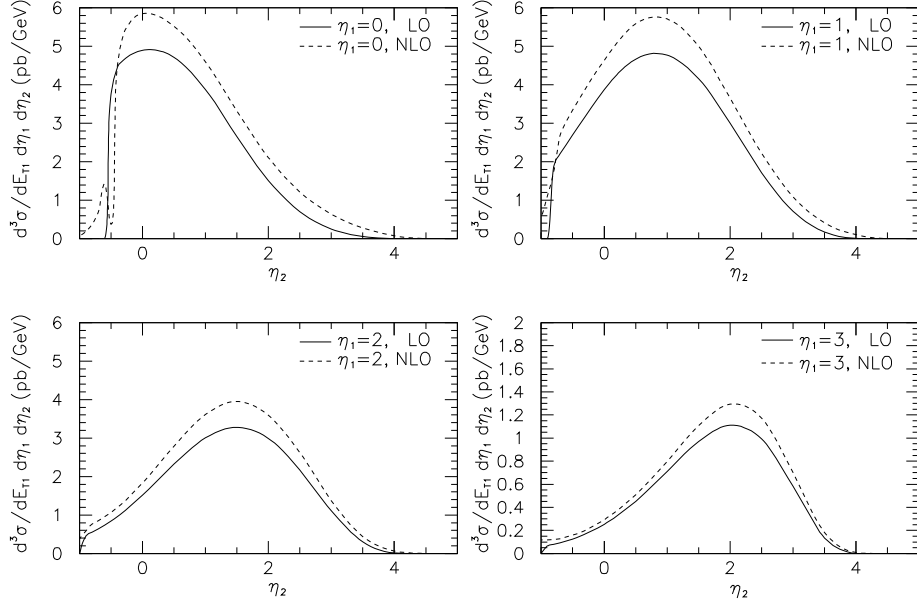


Figure 3: Projections of the LO (full curves) and NLO (dashed curves) triple differential dijet cross section for direct photons at  $E_{T_1} = 20$  GeV and fixed values of  $\eta_1 = 0, 1, 2,$  and  $3,$  as a function of  $\eta_2$ .

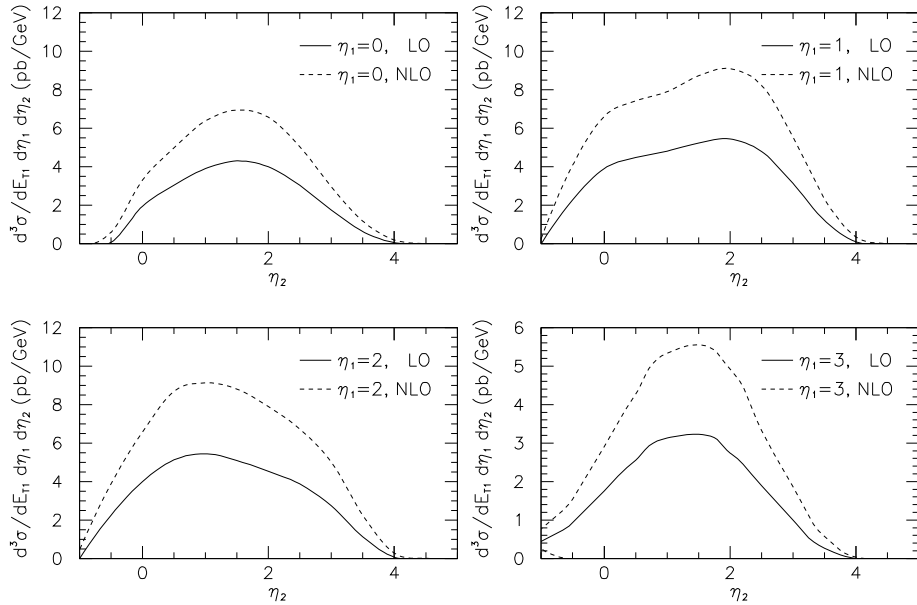


Figure 4: Projections of the LO (full curves) and NLO (dashed curves) triple differential dijet cross section for resolved photons at  $E_{T_1} = 20$  GeV and fixed values of  $\eta_1 = 0, 1, 2,$  and  $3,$  as a function of  $\eta_2$ .

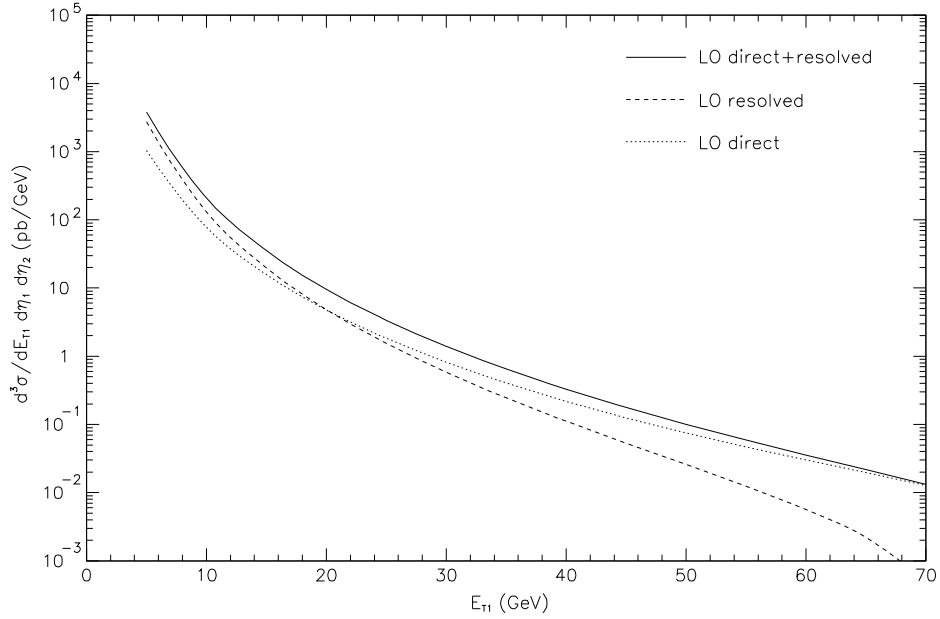


Figure 5: *Inclusive dijet cross section  $d^3\sigma/dE_{T_1}d\eta_1d\eta_2$  for full photoproduction at  $\eta_1 = \eta_2 = 1$  as a function of  $E_{T_1}$ . The full curve is the sum of the LO direct (dotted) and LO resolved (dashed) contributions.*

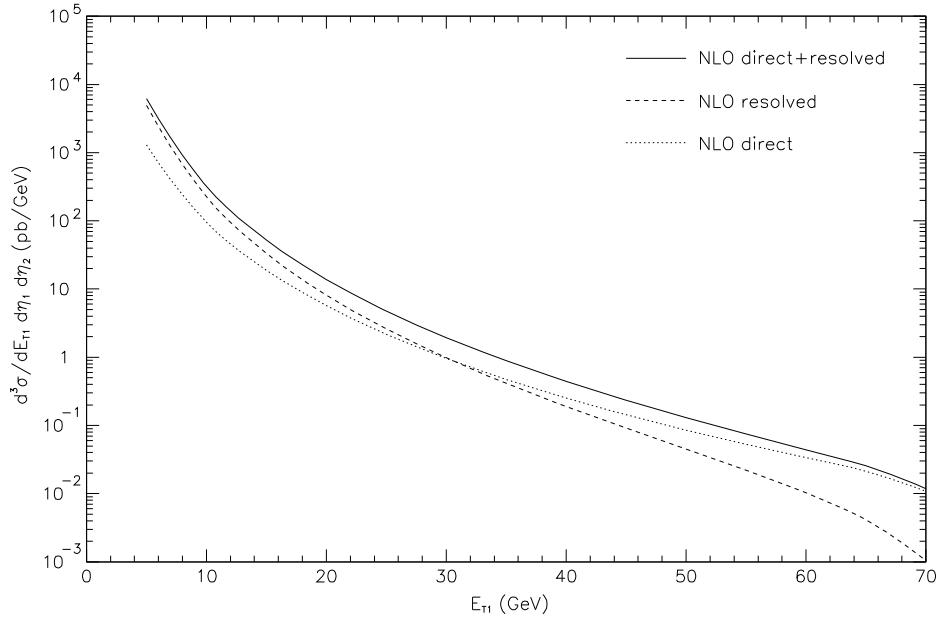


Figure 6: *Inclusive dijet cross section  $d^3\sigma/dE_{T_1}d\eta_1d\eta_2$  for full photoproduction at  $\eta_1 = \eta_2 = 1$  as a function of  $E_{T_1}$ . The full curve is the sum of the NLO direct (dotted) and NLO resolved (dashed) contributions.*

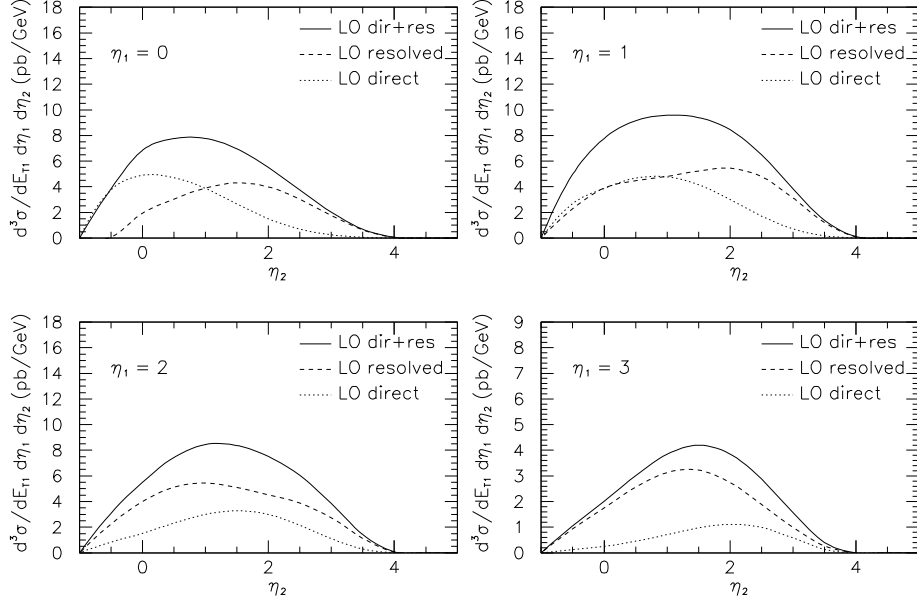


Figure 7: Projections of the complete triple differential dijet cross section at  $E_{T_1} = 20$  GeV and fixed values of  $\eta_1 = 0, 1, 2,$  and  $3,$  as a function of  $\eta_2$ . The full curve is the sum of the LO direct (dotted) and LO resolved (dashed) contributions.

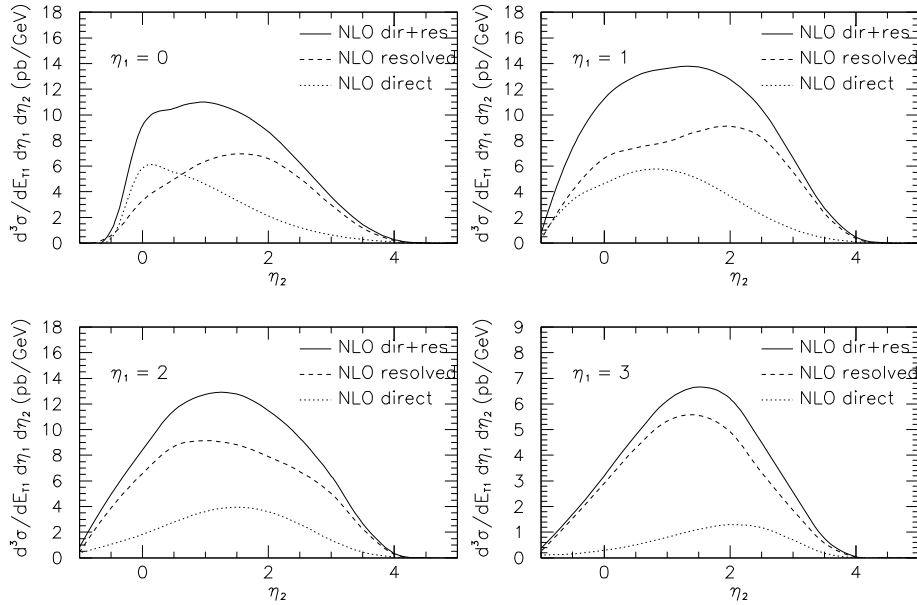


Figure 8: Projections of the complete triple differential dijet cross section at  $E_{T_1} = 20$  GeV and fixed values of  $\eta_1 = 0, 1, 2,$  and  $3,$  as a function of  $\eta_2$ . The full curve is the sum of the NLO direct (dotted) and NLO resolved (dashed) contributions.

and resolved processes changes when calculating dijet photoproduction in next-to-leading order  $\mathcal{O}(\alpha_s^2)$ : resolved processes are much more important at  $E_{T_1} = 20$  GeV than one would have guessed from a leading order estimate.

For the comparison of our two-jet predictions with experimental data it is essential that for the theoretical calculations the same jet definitions are introduced as used in the experimental analysis. First experimental data for inclusive two-jet production have been published by the ZEUS collaboration in [7] and [18]. The analysis of these data was based on the usual cone algorithm with  $R = 1$  [12] similar to the cone algorithm which we used in our NLO calculations presented above. The recent ZEUS analysis [11] based on the 1994 data taking extends the earlier analysis [7] based on the 1993 data in several ways. The larger integrated luminosity utilized in 1994 lead to a reduction of the statistical errors as well as allowing for the measurement of the cross section at higher  $E_T$ , a region, where uncertainties due to non-perturbative hadronization of partons into jets are expected to be reduced making the comparison with the NLO predictions more meaningful. Furthermore, the ZEUS collaboration applied three different jet definitions: two variations of the cone algorithm [12] are used which they called “EUCCELL” and “PUCELL”. These algorithms treat seed finding and jet merging in different ways. In addition, the  $k_T$  cluster algorithm “KTCLUS” [19] for hadron-hadron collisions is used. In [19], several versions of the  $k_T$  algorithm have been introduced which left some flexibility about how the stopping condition and the recombination scheme can be implemented. A version which is particularly suitable to define jets for inclusive jet cross section measurements was emphasized in [20]. It is also closest to the cone algorithms and states that two protojets  $i$  and  $j$  (i.e. two partons in the three parton final states) are merged if

$$\sqrt{(\eta_i - \eta_j)^2 + (\phi_i - \phi_j)^2} < 1 \quad (6)$$

and the recombination of the two protojets is done with the  $E_T$  scheme as is usually also done in the cone algorithms [12]. Compared to the cone algorithm [12] with  $R = 1$ , which was applied so far to generate the results in figs. 1-8, the two partons are merged if they are less than  $R = 1$  apart in  $\eta - \phi$  space, whereas in the cone algorithm the merging condition is on the opening angle between either of the two partons and the jet center obtained from the  $E_T$  recombination equations, i.e.  $R_i < R$  and  $R_j < R$  with  $R = 1$  and  $R_i$  defined in equation (5). Thus this version of the  $k_T$  algorithm is very similar to the cone algorithm usually applied in hadron-hadron and photon-hadron collision. As it is a cluster algorithm, the ambiguities associated with seed finding and jet merging are avoided. The same  $k_T$  algorithm, denoted by KTCLUS, was used by the ZEUS collaboration in the analysis of their recent data [11].

Except for the different jet definition, the cross section to be compared to the ZEUS data is the same as in our earlier work [6]. It is the inclusive two-jet cross section  $d^3\sigma/dE_T d\bar{\eta} d\eta^*$ , where  $\bar{\eta} = \frac{1}{2}(\eta_1 + \eta_2)$  is the average rapidity of the two observed jets and  $E_T$  is the transverse energy of the “trigger” jet. This cross section is integrated over the difference in rapidity,  $|\eta^*| < 0.5$ , and integrated over  $E_{T_1}, E_{T_2} > E_T^{\min}$  with varying  $E_T^{\min}$ . The additional restrictions on the individual rapidities  $\eta_1$  and  $\eta_2$  used in the ZEUS analysis have not been implemented since they only modify the cross sections at  $\bar{\eta} \simeq 2$ . As the experimental constraint on the transverse energies of both jets is not infrared safe in NLO, we allow the second jet to have a transverse energy less than  $E_T^{\min}$  if the third unobserved jet is soft, i.e. has a transverse energy of less than 1 GeV ( $E_{T_3} < 1$  GeV). Through this procedure we avoid the dependence of the theoretical prediction on the  $y$ -cut. In addition, we separate “direct” and “resolved” contributions with

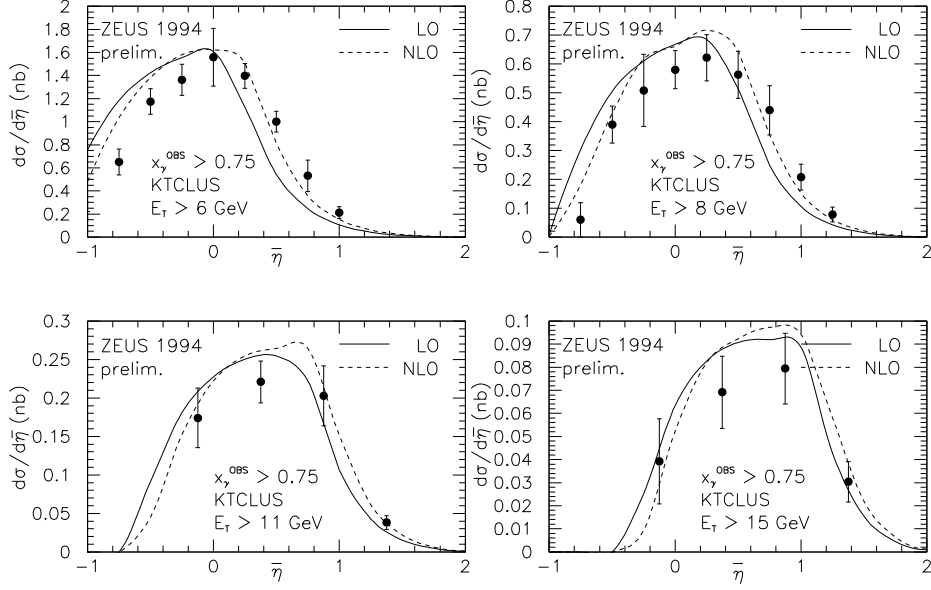


Figure 9: *Inclusive dijet cross section  $d\sigma/d\bar{\eta}$  at  $x_\gamma^{\text{OBS}} > 0.75$  as a function of  $\bar{\eta}$  and integrated over  $\eta^* \in [-0.5, 0.5]$  and  $E_T > 6, 8, 11,$  and  $15$  GeV. Our leading and next-to-leading order predictions are compared to preliminary 1994 data from ZEUS using the KTCLUS algorithm.*

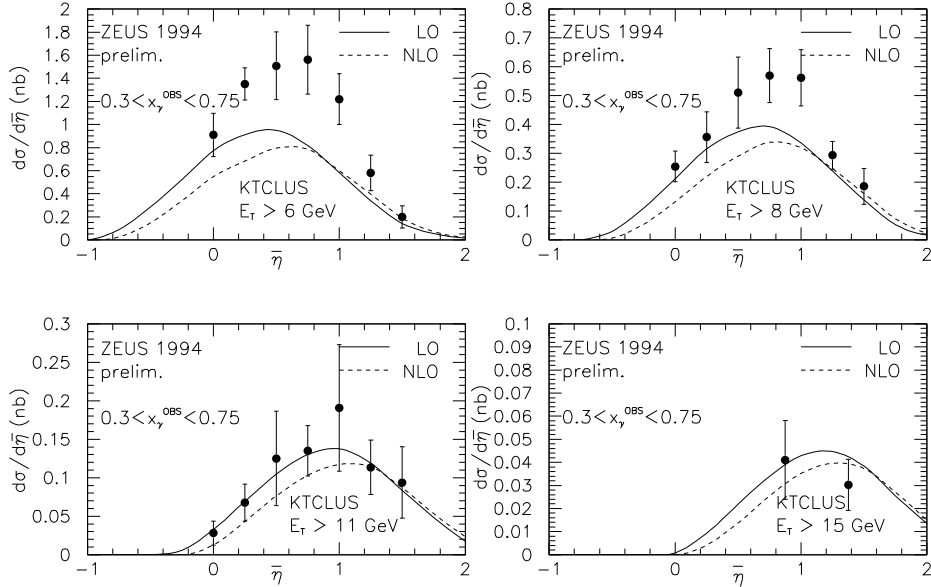


Figure 10: *Inclusive dijet cross section  $d\sigma/d\bar{\eta}$  at  $x_\gamma^{\text{OBS}} \in [0.3, 0.75]$  as a function of  $\bar{\eta}$  and integrated over  $\eta^* \in [-0.5, 0.5]$  and  $E_T > 6, 8, 11,$  and  $15$  GeV. Our leading and next-to-leading order predictions are compared to preliminary 1994 data from ZEUS using the KTCLUS algorithm.*

the variable

$$x_\gamma^{\text{OBS}} = \frac{\sum_i E_{T_i} e^{-\eta_i}}{2x_a E_e}, \quad (7)$$

which measures the fraction of the photon energy that goes into the production of the two hardest jets. As in the ZEUS analysis the enriched direct  $\gamma$  sample is defined with the cut on  $x_\gamma^{\text{OBS}} > 0.75$ . The enriched resolved  $\gamma$  sample is obtained for  $0.3 < x_\gamma^{\text{OBS}} < 0.75$ . The very low  $x_\gamma^{\text{OBS}}$  are excluded in the experimental analysis since this region is not accounted for by the Monte Carlo routines necessary to correct for detector effects. Fig. 9 shows the “direct” cross sections  $d\sigma/d\bar{\eta}$  as a function of  $\bar{\eta}$  in LO and in NLO for  $E_T^{\text{min}} = 6, 8, 11, \text{ and } 15$  GeV together with the preliminary ZEUS data [11]. The LO and NLO predictions are very similar. We emphasize that the LO curve is calculated with the same NLO structure functions as in the NLO calculations, only the hard scattering parton-parton cross sections are evaluated in LO. The NLO curves are shifted to larger  $\bar{\eta}$  and agree in average better with the data than the LO curves. The general agreement is quite good indicating that the GRV choice for the photon parton distributions needed for the resolved contribution is quite reasonable in the high  $x_\gamma$  region. In our previous publication [6], we compared the corresponding 1993 ZEUS data to our prediction, which then only included the LO resolved contributions for the GRV photon parton densities.

The “resolved” photon two-jet cross section, where  $0.3 < x_\gamma^{\text{OBS}} < 0.75$ , is compared to the ZEUS data in fig. 10 for the same  $E_T^{\text{min}}$  values. Here the agreement is satisfactory only with the data in the high  $E_T$  regions  $E_T^{\text{min}} = 11$  and 15 GeV. At the lower  $E_T$ , the experimental cross section is larger than the NLO prediction. The disagreement increases with decreasing  $E_T^{\text{min}}$ . We attribute this difference between theory and experimental data to additional contributions due to multiple interactions with the remnant jet not accounted for by our NLO predictions. As one would expect that these effects diminish with increasing  $E_T$ , the agreement between theory and experiment improves in the large  $E_T$  region. We also studied the uncertainty coming from the insufficiently constrained gluon in the photon by recalculating the resolved cross section with twice the GRV gluon distribution. At low  $E_T$ , the cross section is enhanced by 33% thus reducing the discrepancy, whereas at large  $E_T$  it is only enhanced by 20%. With more accurate data at  $E_T > 17$  GeV, such a gluon distribution could be excluded. In addition to the experimental errors shown, which include systematic and statistical errors added in quadrature, there is a systematic uncertainty arising from the uncertainty in the calorimeter energy scale, which is highly correlated between bins and is therefore excluded from the systematic errors shown in figs. 9 and 10. This uncertainty is largest for the “resolved” cross section at  $E_T^{\text{min}} = 6$  GeV and leads to a  $\pm 0.5$  nb uncertainty in the cross section near  $\bar{\eta} \simeq 0.6$  [11]. In the “direct” cross section, this energy scale uncertainty is smaller by a factor of two [11].

In fig. 10, we observe that the NLO two-jet cross sections are somewhat smaller than the LO cross sections, which are included only to see the effect of the NLO corrections. These LO cross sections are independent of the jet definition, i.e. are always the same for the cluster algorithm or a cone algorithm with any cone radius. They should not be compared to the experimental data since it is known that the two-jet cross sections depend on the jet definitions. The choice of the jet definition has an effect of about 25-30% in both data and theory in the “direct” cross section and of about 50% for the “resolved” cross section [11, 21].

## 4 Summary

Differential cross sections  $d^3\sigma/dE_T d\eta_1 d\eta_2$  have been calculated in NLO for direct and resolved photoproduction. Infrared and collinear singularities are cancelled with the phase space slicing method using an invariant mass cut-off. With this method we are able to incorporate various cuts on the final state as used in the analysis of experimental data and to perform calculations for different choices of jet algorithms. Numerical results for the two-jet inclusive cross sections at HERA have been presented employing the usual Snowmass cone algorithm for the jet definition. For a cone radius of  $R = 1$ , the NLO corrections lead to an increase of the order of 70% compared to the LO prediction in the resolved contribution and of the order of 20% in the direct case already presented earlier [8].

Using a particular version of the  $k_T$  cluster algorithm [20], we calculated the cross section  $d\sigma/d\bar{\eta}$  with cuts on  $x_\gamma^{\text{OBS}}$  to separate “direct” and “resolved” contributions as in the analysis of the ZEUS data [7, 11, 18]. We find fairly good agreement with recent ZEUS data [11] for the enriched direct  $\gamma$  sample. For the enriched resolved  $\gamma$  sample, the agreement is good in the larger  $E_T$  region,  $E_T^{\text{min}} \geq 11$  GeV. For smaller  $E_T$  ( $E_T^{\text{min}} = 6$  and 8 GeV), we find a discrepancy which we attribute to additional multi-parton interactions [11] not incorporated in the theoretical calculations.

## Acknowledgements

It is a pleasure to thank J. Butterworth and L. Feld for valuable discussions on the ZEUS dijet analysis.

## References

- [1] L.E. Gordon, J.K. Storrow, Phys. Lett. **B291** (1992) 320.
- [2] S.G. Salesch, Ph.D. thesis, University of Hamburg, Hamburg, DESY 93-196 (1993),  
G. Kramer, S.G. Salesch, Z. Phys. **C61** (1994) 277,  
M. Klasen, G. Kramer, S.G. Salesch, Z. Phys. **C68** (1995) 113.
- [3] P. Aurenche, M. Fontannaz, J.P. Guillet, Phys. Lett. **B338** (1994) 98.
- [4] M. Derrick et al., ZEUS Collaboration, Phys. Lett. **B342** (1995) 417.
- [5] A. Bouniatian, Ph.D. Thesis, University of Hamburg, Hamburg, DESY FH1K-95-04 (1995),  
S. Aid et al., H1 Collaboration, Z. Phys. **C70** (1996) 17.
- [6] M. Klasen, G. Kramer, Phys. Lett. **B366** (1996) 385.
- [7] M. Derrick et al., ZEUS Collaboration, Phys. Lett. **B348** (1995) 665.
- [8] M. Klasen, G. Kramer, Z. Phys. **C72** (1996) 107.
- [9] M. Klasen, Ph.D. thesis, University of Hamburg, Hamburg, DESY 96-204 (1996).

- [10] M. Klasen, T. Kleinwort, G. Kramer, in preparation.
- [11] M. Derrick et al., ZEUS Collaboration, Talk given at XXVIII International Conference on High Energy Physics, Warsaw (1996).
- [12] J.E. Huth et al., Proc. of the 1990 DPF Summer Study on High Energy Physics, Snowmass, Colorado, edited by E.L. Berger, World Scientific, Singapore (1992) 134.
- [13] T. Kleinwort, Ph.D. thesis, University of Hamburg, Hamburg, DESY 96-195 (1996).
- [14] S.G. Salesch, H1 internal note H1-05/95-441, unpublished (1995).
- [15] D. Bödeker, G. Kramer, S.G. Salesch, Z. Phys. **C63** (1994) 471.
- [16] M. Glück, E. Reya, A. Vogt, Phys. Rev. **D46** (1992) 1973.
- [17] H.L. Lai, J. Botts, J. Huston, J.G. Morfin, J.F. Owens, J.W. Qiu, W.K. Tung, H. Weerts, Phys. Rev. **D51** (1995) 4763.
- [18] M. Derrick et al., ZEUS Collaboration, Phys. Lett. **B384** (1996) 401.
- [19] S. Catani, Yu.L. Dokshitzer, M.H. Seymour, B.R. Webber, Nucl. Phys. **B406** (1993) 187.
- [20] S.D. Ellis, D.E. Soper, Phys. Rev. **D48** (1993) 3160. See also:  
M.H. Seymour, Proceedings of the 10<sup>th</sup> Topical Workshop on “Proton-Antiproton Collider Physics”, edited by R. Raja and J. Yoh, Batavia, IL (1995).  
M.H. Seymour, private communication.
- [21] J.M. Butterworth, L. Feld, M. Klasen, G. Kramer, in: “Future Physics at HERA”, Proceedings of the Workshop 1995/96, edited by G. Ingelman, A. De Roeck, and R. Klanner, DESY, Hamburg (1996), Vol. 1, p. 554, hep-ph/9608481.